Available online at www.sciencedirect.com
SCIENCE DIRECT
Biochemical and Biophysical Research Communications 338 (2005) 1059–1064
BBRC
www.elsevier.com/locate/ybbrc

Theoretical studies of Alzheimer's disease drug candidate 3-[(2,4-dimethoxy)benzylidene]-anabaseine (GTS-21) and its derivatives

Dong-Qing Wei [a,b,e,*], Suzane Sirois [c,e], Qi-Shi Du [a,e], Hugo R. Arias [d], Kuo-Chen Chou [a,e,*]

[a] *Tianjin Institute of Bioinformatics and Drug Discoveries, Tianjin Normal University, Tianjin 300074, China*
[b] *Center for Research on Molecular Modeling, Concordia University, Montreal, Canada*
[c] *Chemistry Department, Université du Québec à Montréal (UQAM), C.P. 8888 Succursale Centre-Ville, Montréal, Que., Canada H3C 3P8*
[d] *Department of Pharmaceutical Sciences, College of Pharmacy, Western University of Health Sciences, Pomona, CA 91766-1854, USA*
[e] *Gordon Life Science Institute, 13784 Torrey Del Mar Drive, San Diego, CA 92130, USA*

Received 22 September 2005
Available online 21 October 2005

Abstract

Theoretical and molecular modeling studies have been conducted for understanding the details of how 3-[(2,4-dimethoxy)benzylidene]-anabaseine dihydrochloride (GTS-21) and its metabolism derivatives bind with the receptor of α7 nicotinic acetylcholine dimer. Good accordance with experimental results has been achieved. It was found that the van der Waals repulsion makes the dominant contribution to the binding energy. GTS-21 and its metabolites are apparently too large for the binding sites of the α7 dimer. To improve the effectiveness of the drug, a possible approach is to reduce its volume while maintaining the presence of the active groups. Our studies, in combination with experimental studies, will lead to a promising basis for practical drug design against Alzheimer's disease.

Keywords: Alzheimer's Disease; GTS-21; α7 Nicotinic acetylcholine receptor; Molecular modeling; Docking; Structural bioinformatics

Nicotine produces its actions on mammalian tissue via interactions with a family of ligand-gated ion channels [1–3] that modulate the effects of the alkaloid on nervous, cardiovascular, immune, and neuromuscular system function. The neuronal nicotinic acetylcholine receptors (nAChRs) are named on the basis of their subunit components, e.g., α4β2, and are thought to have a pentameric functional motif formed from a variety of subunits that comprise an ion channel similar to that of the neuromuscular junction nAChR. Two of the most abundant brain nAChRs are the heteromeric α4β2 and homomeric α7 subtypes. The former contributes 90% of the high-affinity binding sites for nicotine in the rat brain [4]. The low-nicotine-affinity α7 nAChR is recognized by its nanomolar affinity for bungarotoxin [5]. These two widely distributed brain nAChR subtypes occur in cortical and hippocampal neurons involved in cognitive functions. Other brains, autonomic ganglia, and skeletal muscle nAChRs are composed of different subunit combinations [6,7]. Decreases in the low-nicotine-affinity α7-type receptors were very small in the postmortem brains of patients with Alzheimer's disease [8]. However, it has been suggested that the α7 nAChR is an important target for β-amyloid-mediated neurotoxicity [9]. β-Amyloid 1–42 activation of α7 receptors expressed in the *Xenopus laevis* oocyte was prevented by two α7 ligands, the antagonist methyllycaconitine and a metabolite of GTS-21, which is a focus of this article [10]. The α7 receptor agonists enhance cognition and auditory-gating processes and thus are attractive drug candidates for the treatment of senile dementias and schizophrenia [11–13].

For many proteins that are important for drug design but are often difficult to be timely determined by means of X-ray crystallography and NMR techniques, structural bioinformatics can play an important complementary role

* Corresponding authors.
E-mail addresses: lifescience@san.rr.com (D.-Q. Wei), kchou@san.rr.com (K.-C. Chou).

0006-291X/$ - see front matter © 2005 Elsevier Inc. All rights reserved.
doi:10.1016/j.bbrc.2005.10.047

in this regard [14–16,36,37], particularly for transmembrane proteins [17–19]. Although the 3D structures derived by structural bioinformatics are not as accurate as X-ray ones, they can provide many important insights into drug design [20–28].

Recently, based on the crystal structure of acetylcholine-binding protein, or AChBP (1i9b), the three-dimensional structures of the extracellular domain (or the ligand-binding domains) of the monomer, homodimer, and homopentamer of the α7 nAChR were derived [17]. The interface between two subunits, where the ligand-binding site is located, was investigated. Furthermore, an explicit definition of the ligand-binding pocket was illustrated that might provide useful clues for conducting various mutagenesis studies for finding drugs against schizophrenia and Alzheimer's disease. The current study is a preliminary docking study of GTS-21 and its derivatives with respect to the newly available 3D structures of α7 nAChR.

Until very recently, few selective ligands were available with which to study nAChR function beyond nicotine itself and several other compounds such as cytisine, DHbE, mecamylamine, and chlorisodamine. Medicinal and natural product chemistry efforts over the past decade have, however, expanded considerably on this limited repertoire with the identification of a number of nicotine bioisosteres and natural products [2], some of which have been advanced to clinical trials. As these newer compounds are being evaluated in more sophisticated molecular systems, it is becoming increasingly clear that a single molecule can have multiple pharmacologies. Thus, a full agonist at one receptor subtype does not necessarily predict that a compound will be inactive or weakly active at another nAChR. Thus, partial agonists may have full antagonist activity at some subtypes.

GTS-21 [13,29] is a selective α7 nAChR partial agonist in clinical development at Taiho to treat Alzheimer's disease and schizophrenia. GTS-21 was isolated from the nemertine worm *Amphiporus lactifloreus*. The compound has been shown to improve learning performance and memory retention in passive avoidance models in nucleus basalis magnocellularis (NBM)-lesioned rats as well as in active avoidance models in aged rats. It also reduced neocortical cell loss in NBM-lesioned rats and cell death induced by β-amyloid or glutamate in cultures of neuronal cells.

Computational methods

In our docking studies, the ligand is flexible, i.e., the program generates a diversified set of conformations by making random changes to the ligand coordinates [30,31]. While the macromolecular target remains to be rigid, which is a strategy the most docking programs adapt. It ignores the flexibility of the side-chain while the ligand could induce some structural re-arrangement such as hinge binding. Frequently, these changes are minimal, but in some cases, changes in structure upon ligand binding are integral to the function of protein, such as allosteric regulation and signal transductions. When a new conformation of the ligand is generated, the search for favorable binding configurations is conducted within a specified 3D docking box, using either simulated annealing or Tabu search. Both methods seek to optimize the purely spatial contacts as well as electrostatic interactions. The interaction energy is calculated using electrostatic and van der Waals potential fields. In all our computations, the CHARMM22 [32] force field parameters were used.

The docking [30,31] studies were made with respect to the α7 nAChR dimer [17]. The dimer interface is formed by an interlocking array of A- and B-chain elements, which consists of 31 residues, of which 17 are from A-chain and 14 from B-chain (see Table 1 of [17]).

Results and discussions

The Hepes ligand, i.e., 4-(2-hydroxyethyl)-1-piperazine-ethanesulfonic acid, is a very common ligand found in many PDB entries. It is useful to identify the binding pocket for the ligand as reported in [17]. The constituents of the pocket were defined by those residues that have at least one heavy atom (i.e., an atom other than hydrogen) with a distance 5 Å [21,26] from a heavy atom of the Hepes ligand. The pocket thus defined consists of 14 residues, of which eight are from A-chain and six from B-chain. Those from A-chain are Tyr-93A, Ser-148A, Trp-149A, Ser-150A, Tyr-188A, Cys-190A, Cys-191A, and Tyr-195A; and those from B-chain are Trp-55B, Val-108B, Val-110B, Gln-117B, Tyr-118B, and Leu-119B. As shown in Fig. 1A, there are two hydrogen bonds holding the Hepes ligand with the dimer: one is between a sulfonate oxygen of the ligand

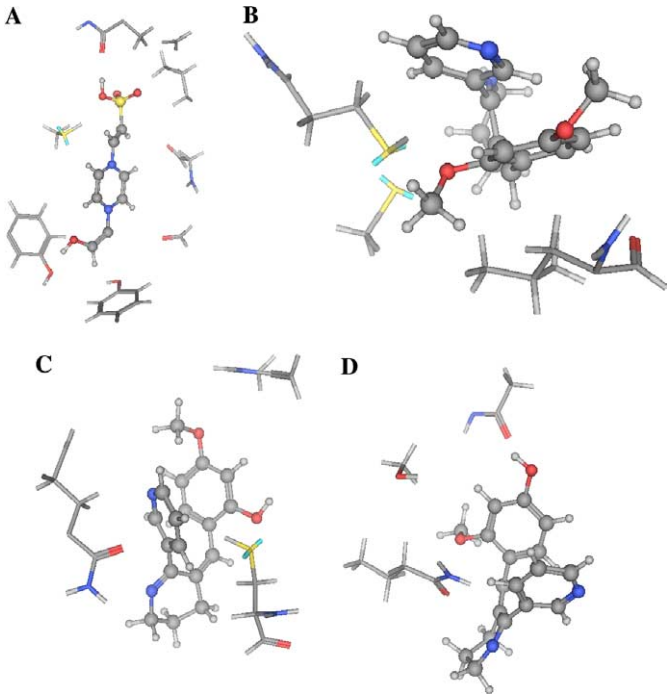

Fig. 1. A close view of the binding site of the ligands. The molecule with the ball-stick representation is the ligand, some residues of the receptor close to the ligand are with stick representation, where the red, gray, blue, yellow, and light-gray colors represent oxygen, carbon, nitrogen, sulfur, and hydrogen, respectively. Panels A–D refer to diagrams aligned from left to right, top to bottom, corresponding to binding of Hepes, GTS-21, 2-OH-GTS-21, and 4-OH-GTS-21 with residues of the receptor, respectively. (For interpretation of the references to color in this figure legend, the reader is referred to the web version of this paper.)

and H(S) of Cys-191A (2.22 Å), and the other is between a hydrogen atom linked to the same sulfonate oxygen and O of Gln-117B (1.71 Å). The latter bond is significantly shorter than the normal hydrogen bond because of the cooperative effect (enhancement) [33] of the first hydrogen bond. Another possible hydrogen bond is between the ligand hydroxyl hydrogen and the hydroxyl oxygen of Tyr-188A. The distance is 2.39 Å. The ligand could move quite freely in the pocket due to its volume, because it is much smaller than the dimension of the pocket.

Fig. 1B is a close look at the ligand GTS-21 in close contact with the receptor, some residues are not shown in the figure to achieve clear view. There are quite a few hydrogen bonds formed between the residues in the pocket, for example, between Leu-119B and Cys-190A and Lys-192A. Weak hydrogen bonds could be formed between the oxygen on two O–CH_3 units and H(S) of Lys-192A and H(N) of Leu-119B, respectively. But in the docked structure, only one is considered to be a hydrogen with a H–O distance of about 2.0 Å, i.e., between O(CH_3) of the ligand and H(S) of Lys-192A. The GTS-21 ligand is significantly larger than Hepes. In fact, it is quite hard to move it around in the pocket. Therefore, the docking energy is dominated by the van der Waals repulsion term.

Because of that 4-OH-GST21 and 2-OH-GTS-21 are more polar than GTS-21, that HO is a very strong proton donor, and that O of OH can also be a good proton acceptor, it should have a better chance to form hydrogen bonds with the receptor. The most energetically favorable docking results are shown in Fig. 1C and D, respectively. Oddly, we do not find any hydrogen bond for 4-OH-GTS-21 although the possibility is certainly there. For 2-OH-GTS-21 there is a hydrogen bond between the O(H) on the ligand and H(S) of Cys-191B(2.16 Å). As shown in Table 1, 4-OH-GTS-21 has the lowest binding energy even though there are no hydrogen bonds formed. This is because the van der Waals repulsion dominates the interaction, which has much to do with the volume of the ligands and that 4-OH-GTS-21 has a smaller volume.

As it is shown in Fig. 2, 2-OH-GTS-21 finds a lower energy position that is aligned somewhat perpendicular to HEP inhibitor, leaving enough room to host the ligand and reduce the van de Waals repulsion. Accordingly, for modifying the ligand to achieve better binding, the volume and alignment of the ligand is of important consideration.

Table 1
Docking energies of various ligands to the α7 receptor (kcal/mol)

Ligands	U_{total}	$U_{binding}$	U_{ligand}
GTS-21	195.33	95.62	99.71
4-OH-GTS-21	111.87	40.81	71.06
2-OH-GTS-21	177.20	101.98	75.22
GTS-21[H^+]	178.62	86.74	91.87
4-OH-GTS-21[H^+]	132.84	58.29	74.55
2-OH-GTS-21[H^+]	97.11	36.01	63.01

U_{total}, $U_{binding}$, and U_{ligand} are the total energy, binding energy, and ligand self-energy, respectively, and $U_{total} = U_{binding} + U_{ligand}$.

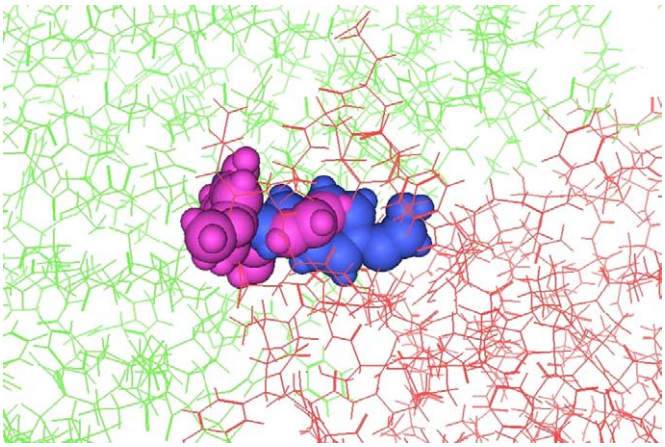

Fig. 2. A distant view of the ligands in the binding pocket. The red and green colors represent the chains A and B, respectively, purple and blue refer to the 2-OH-GTS-21 and HEP, respectively. (For interpretation of the references to color in this figure legend, the reader is referred to the web version of this paper.)

Figs. 3A–C show results of the most favorable docking conformations of GTS-21[H^+], 2-OH-GTS-21[H^+], and 4-OH-GTS-21[H^+] together with some of its near-by residues. It is believed that a significant portion of the GTS-21 molecules are protonated, i.e., acts as a base to react with a proton from water and the protonated ligand binds better with the receptor. As shown in Fig. 3A, more hydrogen bonds are formed for GTS-21[H^+]. Also, H(N) of Trp-149A forms hydrogen bond with both the ligand (2.54 Å) and PRO-120B (1.67 Å). The length of hydrogen bond for the latter is very short, which is due to the cooperative effect of hydrogen bonds [33]. The H^+(N) of the ligand forms a hydrogen bond with Gln-117B (2.30Å). For 2-OH-GTS-21[H^+] and 4-OH-GTS-21[H^+], each has more than two hydrogen bonds. For 2-OH-GTS-21[H^+], there are a few possible hydrogen bonds; e.g., the hydrogen bonds between O(CH_3) of the ligand and the two H(N) of Glu-193B (2.70 and 2.81 Å, respectively), those of the hydroxyl group of the ligand with H(S) of Cys-191A (2.86 Å) and O(C) of Cys-190A (2.87 Å) respectively, and those of the proton H^+(N) of the ligand with O(H) of Ser-150A (3.49 Å). For 4-OH-GTS-21[H^+], two hydrogen bonds are found: one is between O(CH_3) of the ligand and H(S) of Cys-191A (2.43 Å), and the other between hydroxyl H(O) and Gln-117B (2.07 Å). Adding a positively charged proton to the ligand will certainly create opportunity for the ligand to bind favorably with the residues of the receptor because many residues have readily available proton acceptors, for example, Gln-117B and Ser-150A. The presence of the positive charge makes the hydrogen bond stronger or promotes formation of the "strong" hydrogen bonds (barrierless) [33].

From Table 1, we see that 2-OH-GTS-21[H^+] has the best binding energy (lowest). However as it is shown in Fig. 3C, it does not really have a lot of hydrogen bonds. As it is the case of unprotonated 4-OH-GTS-21, the van der Waals interaction is the key factor in determining the

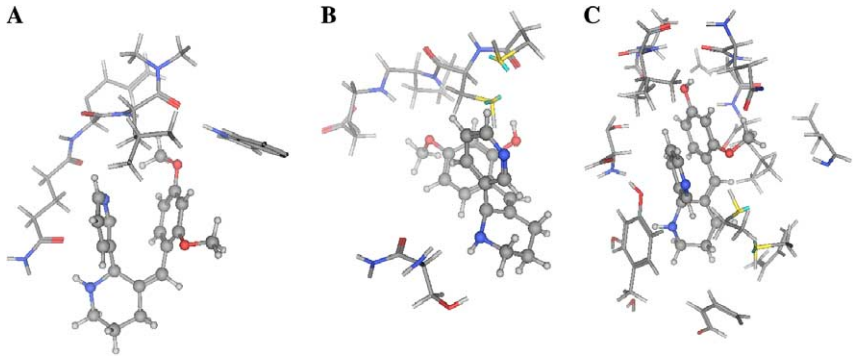

Fig. 3. The binding pocket of GTS-21[H^+] and its derivatives. The molecule with the ball-stick representation is the ligand. Residues of the receptor close to the ligand are with stick representation, where the red, gray, blue, yellow, and light-gray colors represent oxygen, carbon, nitrogen, sulfur, and hydrogen, respectively. Panels A–C refer to diagrams aligned from left to right, top to bottom, corresponding to binding of GTS-21[H^+], 2-OH-GTS-21[H^+], and 4-OH-GTS-21[H^+] with residues of the receptor, respectively. (For interpretation of the references to color in this figure legend, the reader is referred to the web version of this paper.)

binding energy. We have made a plot of the molecular surface [34,35] of the residues close to the 2-OH-GTS-21[H^+] as shown in Fig. 4A. We find that there are good matches between the hydrophobic and hydrophilic areas between the receptor and the ligand. We could understand why the energy is dominated by van der Waals repulsion from Fig. 4A: the van der Waals surface of the ligands penetrates the molecular surface of the receptor. It indicates that the pocket space is not large enough to allow the ligand stay comfortably, and hence the ligands push its way to the territory of the receptor. Fig. 4B gives a sense of the shape of the ligand GTS-21-4OH[H^+] and its hydrophobicity. It would be useful for future design of the new ligand.

In our docking studies, we choose the ligand conformation with the lowest total energy as the most favorable binding conformation. The total energy is consists of three parts: the electrostatic, van der walls, and ligand energies. Among the lowest total energy conformations the energy of many ligands is close to that of isolated molecule, i.e., the structure of the low energy conformations is similar to that of the optimized free molecule, which is a close packed structure with the pyridyl and benzyl rings being almost in parallel.

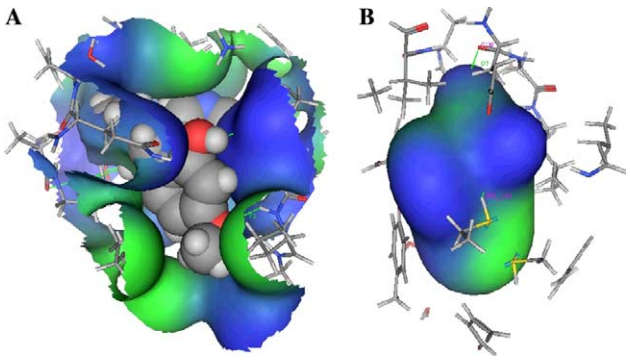

Fig. 4. A close view of the ligand 2-OH-GTS-21[H^+] embedded in the molecular surface of the nearby residues of the receptor and 4-OH-GTS-21[H^+] molecular surface, where the surfaces were rendered with the hydrophobicity attributes, green and blue areas represent hydrophobic and hydrophilic measure, respectively. The ligand is colored according to the atomic types as specified in previous figures. (For interpretation of the references to color in this figure legend, the reader is referred to the web version of this paper.)

Based on Table 1, we can answer the question why 4-OH-GTS-21 has better affinity with the α7 receptor. The stronger binding energy mainly comes from the contribution of van der Waals interaction. According to Kem et al. [29], the ionized form of this ligand has a much higher affinity for the α7 receptor than the unionized form. This is certainly supported by the current docking results, where it is shown that the ligand forms more hydrogen bonds, and both electrostatic and van der Waals interactions are more favorable. In the acid environment, the percentage of 2-OH-GTS-21[H^+] and 4-OH-GTS-21[H^+] is larger and the affinity increases, which also fully agrees with experiments.

It is reported [29] that the preferred conformations of GTS-21 and its metabolites in their neutral and monocationic forms were very similar, derived from their semiempirical (PM5) quantum chemical models, as modeled in water using the COSMO approach. In contrast with the preferred conformation of anabaseine where the two rings are coplanar, in the preferred conformations of the four benzylidene compounds, the two anabaseinoid rings are twisted with respect to each other. Protonation of GTS-21 further increases this angle. The preferred conformations of the three metabolites were not significantly different from those of GTS-21, except for a further twisting (approximately −40°) of the pyridyl ring with respect to the tetrahydropyridyl ring. A geometry optimization was made using the CHARMM22 force field for isolated molecule. It is found that the pyridyl ring is almost parallel to the benzyl ring, two dihedral angles defined in Kem et al.s paper being: −49.3 and −61.7°, respectively, and the N1–N2 and N1–O1 distances being 4.21 and 3.94 Å, respectively, which are quite different from the corresponding values given by Kem et al, i.e., −55.4 and 107.4°, as well as, 4.27 and 5.57 Å. It seems to be essential for the ligand to

Table 2
Molecular parameters of some minimum conformations

	Compounds	N1–N2 (Å)	N1–O1 (Å)	C1–C2–C3–C4 (°)	C1–C5–C6–7 (°)
CHARMM22	GTS-21	4.21	3.94	−49.3	−61.7
in gas phase	GTS-21[H^+]	4.63	3.65	−60.6	−55.4
	2-OH-GTS-21[H^+]	4.64	3.92	−61.5	−62.4
	4-OH-GTS-21[H^+]	4.62	3.62	−60.4	−55.1
Minimum free energy	GTS-21	4.27	5.57	−107.4	−55.4
conformations in	GTS-21[H^+]	4.43	6.38	−124.7	−81.4
water by PM5	2-OH-GTS-21[H^+]	4.64	6.07	−126.8	−123.1
	4-OH-GTS-21[H^+]	4.63	5.85	−125.9	−121.2

be in a compact form to fit into the pocket. The CHARMM structure looks more compact than that of Kem et al. Table 2 gives the structural information of GTS-21 and its protonated derivatives. Further Quantum mechanical studies for isolated molecule and in liquid/enzyme environment are warranted to pursue.

The current docking studies represent very extensive computational efforts. Good accordance with experimental results has been achieved. It is found that the van der Waals repulsion makes the dominant contribution to the binding energy. GTS-21 and its metabolites are apparently too large for the binding sites of α7 dimer. To improve the effectiveness of the drug, one should find ways to reduce its volume while maintaining the presence of the active groups. The results obtained through the current studies, combined with experimental studies, may provide useful insights into drug design against Alzheimer's disease.

Acknowledgments

This work was supported by grants from Chinese National Science Foundation under the Contract No. 10376024 and the Tianjin Commission of Sciences and Technology under the Contract No. 033801911 and special fund for intensive computation.

References

[1] C. Gotti, D. Fornasari, F. Clementi, Human neuronal nicotinic receptors, Prog. Neurobiol. 53 (1997) 199–237.
[2] M.W. Holladay, M.J. Dart, J.K. Lynch, Neuronal nicotinic acetylcholine receptors as targets for drug discovery, J. Med. Chem. 40 (1997) 4169–4194.
[3] J.P. Changeux, D. Bertrand, P.J. Corringer, S. Dehaene, S. Edelstein, C. Lena, N. Le Novere, L. Marubio, M. Picciotto, M. Zoli, Brain nicotinic receptors: structure and regulation, role in learning and reinforcement, Brain Res. Rev. 26 (1998) 198–216.
[4] C.M. Flores, S.W. Rogers, L.A. Pabreza, B.B. Wolfe, K.L. Kellar, A subtype of nicotinic cholinergic receptor in rat brain is composed of α4 and β2 subunits and is up-regulated by chronic nicotine treatment, Mol. Pharmacol. 41 (1992) 31–37.
[5] M.J. Marks, A.C. Collins, Characterization of nicotine binding in mouse brain and comparison with the binding of alpha-bungarotoxin and quinuclidinyl benzylate, Mol. Pharmacol 22 (1982) 554–564.
[6] J. Lindstrom, Neuronal nicotinic acetylcholine receptors, in: T. Narahashi (Ed.), Ion Channels, Plenum Press, New York, 1996, pp. 377–450.
[7] N. Champtiaux, Z.Y. Han, A. Bessis, F.M. Rossi, M. Zoli, L. Marubio, J.M. McIntosh, J.P. Changeux, Distribution and pharmacology of alpha6-containing nicotinic acetylcholine receptors analyzed with mutant mice, J. Neurosci. 22 (2002) 1208–12017.
[8] C.M. Martin-Ruiz, J.A. Court, E. Molnar, M. Lee, C. Gotti, A. Mamalaki, T. Tsouloufis, S. Tzartos, C. Ballard, R.H. Perry, et al., Alpha4 but not alpha3 and alpha7 nicotinic acetylcholine receptor subunits are lost from the temporal cortex in Alzheimer's disease, J. Neurochem. 73 (1999) 1635–1640.
[9] H.-Y. Wang, D.H.S. Lee, C.B. Davis, R.P. Shank, Amyloid peptide AB1–42 binds selectively and with picomolar affinity to alpha7 nicotinic receptors, J. Neurochem. 75 (2000) 1155–1161.
[10] K.T. Dineley, K.A. Bell, D. Bui, J.D. Sweatt, Beta-amyloid peptide activates alpha7 nicotinic acetylcholine receptors expressed in *Xenopus* oocytes, J. Biol. Chem. 277 (2002) 25056–25061.
[11] R. Freedman, L.E. Adler, M. Waldo, M. Myles-Worsley, H.T. Nagamoto, C. Miller, M. Kisly, K. McRae, E. Cawthra, Inhibitory gating of an evoked response to repeated auditory stimuli in schizophrenic and normal subjects: human recordings, computer simulation and an animal model, Arch. Gen. Psychiatry 53 (1996) 1114–1121.
[12] K.E. Stevens, W.R. Kem, V.M. Mahnir, R. Freedman, Selective alpha7-nicotinic agonists normalize inhibition of auditory response in DBA mice, Psychopharmacology (Berl) 136 (1998) 320–327.
[13] W.R. Kem, The brain alpha7 nicotinic receptor may be an important therapeutic target for the treatment of Alzheimer's disease: studies with DMXBA (GTS-21), Behav. Brain Res. 113 (2000) 169–183.
[14] K.C. Chou, Review: structural bioinformatics and its impact to biomedical science, Curr. Med. Chem. 11 (2004) 2105–2134.
[15] J.J. Chou, H. Matsuo, H. Duan, G. Wagner, Solution structure of the RAIDD CARD and model for CARD/CARD interaction in caspase-2 and caspase-9 recruitment, Cell 94 (1998) 171–180.
[16] J.J Chou, H. Li, G.S. Salvessen, J. Yuan, G. Wagner, Solution structure of BID, an intracellular amplifier of apoptotic signaling, Cell 96 (1999) 615–624.
[17] K.C. Chou, Insights from modelling the 3D structure of the extracellular domain of alpha7 nicotinic acetylcholine receptor, Biochem. Biophys. Res. Commun. 319 (2004) 433–438.
[18] K.C. Chou, Insights from modelling three-dimensional structures of the human potassium and sodium channels, J. Proteome Res. 3 (2004) 856–861.
[19] K.C. Chou, Modelling extracellular domains of GABA-A receptors: subtypes 1, 2, 3, and 5, Biochem. Biophys. Res. Commun. 316 (2004) 636–642.
[20] K.C. Chou, The convergence–divergence duality in lectin domains of the selectin family and its implications, FEBS Lett. 363 (1995) 123–126.
[21] K.C. Chou, D.Q. Wei, W.Z. Zhong, Binding mechanism of coronavirus main proteinase with ligands and its implication to drug design against SARS, Biochem. Biophys. Res. Commun. 308 (2003) 148–151 (Erratum: ibid., 2003, Vol. 310, 675).
[22] K.C. Chou, Molecular therapeutic target for type-2 diabetes, J. Proteome Res. 3 (2004) 1284–1288.

[23] K.C. Chou, Modeling the tertiary structure of human cathepsin-E, Biochem. Biophys. Res. Commun. 331 (2005) 56–60.
[24] K.C. Chou, W.J. Howe, Prediction of the tertiary structure of the beta-secretase zymogen, Biochem. Biophys. Res. Commun. 292 (2002) 702–708.
[25] K.C. Chou, D. Jones, R.L. Heinrikson, Prediction of the tertiary structure and substrate binding site of caspase-8, FEBS Lett. 419 (1997) 49–54.
[26] K.C. Chou, K.D. Watenpaugh, R.L. Heinrikson, A model of the complex between cyclin-dependent kinase 5(Cdk5) and the activation domain of neuronal Cdk5 activator, Biochem. Biophys. Res. Commun. 259 (1999) 420–428.
[27] K.C. Chou, A.G. Tomasselli, R.L. Heinrikson, Prediction of the tertiary structure of a caspase-9/inhibitor complex, FEBS Lett. 470 (2000) 249–256.
[28] J. Zhang, C.H. Luan, K.C. Chou, G.V.W. Johnson, Identification of the N-terminal functional domains of Cdk5 by molecular truncation and computer modeling, PROTEINS: Structure Function and Genetics 48 (2002) 447–453.
[29] W.R. Kem, V.M. Mahnir, L. Prokai, R.L. Papke, X. Cao, S. LeFrancois, K. Wildeboer, K. Prokai-Tatrai, J. Porter-Papke, F. Soti, Mol. Pharmacol. 65 (2004) 56–67.
[30] I.D. Kuntz, E.C. Meng, B.K. Shoichet, Structure-based strategies for drug design and discovery, Acc. Chem. Res. 27 (1994) 117–123.
[31] G.M. Morris, D.S. Goodsell, R.S. Halliday, R. Huey, W.E. Hart, R.K. Belew, A.J. Olson, Automated docking using a Lamarckian Genetic Algorithm and empirical binding free energy function, J. Comput. Chem. 19 (1998) 1639–1662.
[32] A.D. MacKerell Jr., D. Bashford, M. Bellott, R.L. Dunbrack Jr., J.D. Evanseck, M.J. Field, S. Fischer, J. Gao, H. Guo, S. Ha, D. Joseph-McCarthy, L. Kuchnir, K. Kuczera, F.T.K. Lau, C. Mattos, S. Michnick, T. Ngo, D.T. Nguyen, B. Prodhom, W.E. Reiher III, B. Roux, M. Schlenkrich, J.C. Smith, R. Stote, J. Straub, M. Watanabe, J. Wiórkiewicz-Kuczera, D. Yin, M. Karplus, All-atom empirical potential for molecular modeling and dynamics studies of proteins, J. Phys. Chem. B 102 (1998) 3586–3616.
[33] H. Guo, D.R. Salahub, Cooperative hydrogen bonding and enzyme catalysis, Angew. Chem. Int. Ed. Engl. 37 (1998) 2985–2990.
[34] M.L. Connolly, Analytical molecular surface calculation, J. Appl. Crystallogr. 16 (1983) 548–558.
[35] M.L. Connolly, Solvent-accessible surfaces of proteins and nucleic acids, Science 221 (1983) 709–713.
[36] K.C. Chou, Insights from modeling the 3D structure of DNA-CBF3b complex, J. Proteome Res. 4 (2005) 1657–1660.
[37] K.C. Chou, Coupling interaction between thromboxane A2 receptor and alpha-13 subunit of guanine nucleotide-binding protein, J. Proteome Res. 4 (2005) 1681–1686.